AIAA JOURNAL
Vol. 49, No. 12, December 2011

Aeronautic Conceptual Design Optimization Method Based on High-Order Singular Value Decomposition

S. de Lucas,* J. M. Vega,† and A. Velazquez‡
Universidad Politécnica de Madrid, 28040 Madrid, Spain

DOI: 10.2514/1.J051133

An optimization method for conceptual design in aeronautics is presented that is based on a genetic algorithm. The various ingredients in the target function are calculated for each individual using surrogates of the associated technical disciplines that are constructed via high-order singular value decomposition and one-dimensional interpolation. These surrogates result from a limited number of computational fluid dynamics calculated snapshots. The resulting method is both flexible and much more computationally efficient than the conventional method based on direct calculation of the target function, especially if a large number of free design parameters and/or tunable modeling parameters are present. The method is illustrated considering a simplified version of the conceptual design of an aircraft empennage.

Nomenclature

$A_{i_1-i_n}$	=	elements of the tensor A
A_S	=	total area of the mean-lines surface
b	=	complexity penalty
c	=	chord
C	=	complexity
c_f	=	skin friction coefficient
$Cl_{\max}$	=	maximum value of the chordwise lift coefficient
$Cl_{\min}$	=	minimum value of the chordwise lift coefficient
$C_{m\alpha}$	=	longitudinal stability derivative
$C_{m\delta}$	=	longitudinal control derivative
$C_{n\beta}$	=	lateral stability derivative
$C_{n\delta}$	=	lateral control derivative
d	=	torsion box width
D	=	drag
h	=	torsion box height
I_x	=	moment of inertia of the torsion box cross section
M	=	bending moment
m	=	complexity exponent
N_i	=	i-th dimension size of the reduced tensor
p	=	pressure
q	=	generic state variable
Q	=	shear force
$q_{\max}$	=	maximum shear flow
Re_m	=	Reynolds number based on the mean aerodynamic chord
s	=	arch length along the generatrix
S_i	=	i-th dimension size of the truncated reduced tensor
S_{TB}	=	mean-lines surface part of the stabilizers that is occupied to the torsion box
T	=	torsor moment
t_{cov}	=	cover (skin plus stringers) equivalent thickness
t_{sp}	=	spars thickness
U, V, W	=	high-order singular value decomposition modes
U_∞	=	freestream velocity
W_A	=	wetted area
x, y, z	=	Cartesian coordinates: x along the fuselage axis, y perpendicular to the fuselage symmetry plane pointing to the right and z contained in the fuselage symmetry plane pointing upward
x_{le}	=	x coordinate of the stabilizers leading edge
x_{te}	=	x coordinate of the stabilizers trailing edge
α	=	angle of attack
$\alpha_p, \beta_q, \gamma_r$	=	singular values of the high-order singular value decomposition
β	=	yaw angle
$\varepsilon_1, \varepsilon_2, \varepsilon_3$	=	weight factors of the optimization function
θ	=	angle between the airfoil plane and the $x-z$ plane
κ	=	curvature of the generatrix
λ_i	=	i-th geometry parameter
μ_i	=	generic parameter or state variable
ρ_∞	=	freestream density
ρ_{cov}	=	skin material density
ρ_S	=	density per unit surface of the stabilizer part that is not torsion box
ρ_{sp}	=	spar material density
σ	=	stress in the upper cover
σ_{adm}	=	admissible stress
τ_{adm}	=	permissible shear stress
φ	=	angle between the tangent to the generatrix and the chordwise section
$\mathbf{\Phi}$	=	objective function

Subscript

ref	=	reference configuration

Superscripts

HTP	=	horizontal tail plane
VTP	=	vertical tail plane

Received 15 December 2010; revision received 11 April 2011; accepted for publication 15 June 2011.

*Ph.D. Student, Aerospace Propulsion and Fluid Mechanics Department, School of Aeronautics. Plaza del Cardenal Cisneros 3; sergio.delucas@upm.es.

†Professor, Applied Mathematics Department, School of Aeronautics. Plaza del Cardenal Cisneros 3; josemanuel.vega@upm.es.

‡Professor, Aerospace Propulsion and Fluid Mechanics Department, School of Aeronautics. Plaza del Cardenal Cisneros 3; angel.velazquez@upm.es.

I. Introduction

NOWADAYS, aircraft conceptual design in industry is evolving along two seemingly contradictory lines. On one hand, the number of design parameters and tunable modeling parameters keeps growing, and on the other, commercial pressure tends to emphasize the need to shorten the time span allocated to the design cycles. The problem is further complicated by the fact that the free/tunable parameters are of a highly multidisciplinary nature. This involves the

need to use different sets of physics/mathematics modeling equations, and also the need to select the fidelity level of both the models themselves and the interactions between them. In this context, it can be said that conceptual design is becoming more and more "mathematized," not only in the description of the different technical modules but, perhaps more acutely, in the optimization method itself.

A rather comprehensive review on the subject of integrated systems engineering in aircraft design has been published in 2006 by Price et al. [1], who describe at some length the basic aspects of aircraft integrated design, including those (such as cost and life cycle) that are not easily amenable to formalization. Concerning the state of the art, the authors conclude that it is currently feasible to integrate aerodynamics, structures, manufacturing, and CAD for reduced cost and reduced lead time. However, they argue that further integration of the life cycle with regard to performance, cost, environmental impact, and safety is still in its infant stage. It is also worth mentioning their opinion that the main challenge still remains to embody the core principles of integrated systems engineering into formalized models and tools.

Multidisciplinary design optimization (one of the practical realizations of integrated systems engineering) is a technical area that has been, and still is, the subject of a large research and development effort. This effort has been disseminated via hundreds of research articles that would be impossible to reference here. Therefore, we will only quote those articles that are somewhat closer to the problem that we deal with. Multiphysics optimization of aircraft design aiming to minimize the environmental impact has been addressed by Antoine and Kroo [2,3]. They considered an optimization platform that linked modules for the different technical disciplines of engine performance, noise, and engine emissions. In [2], the optimizer was based on a Nelder–Mead algorithm [4], while in [3] the authors used a genetic algorithm (GA). Other studies on the practical applications of multidisciplinary optimization have been reported, for example, by Piperni et al. [5] in the field of business jets, Schumacher et al. [6] in the structural design of a regional aircraft wing box, Bower and Kroo [7] in the minimization of cost and emissions over specific route networks, Rao et al. [8] in the conceptual design of a two-seater propeller driven aircraft, Choi et al. [9] in the design optimization of a supersonic jet, and Werner–Westphal et al. [10] in connection with aircraft generated noise evaluation in the preliminary design.

Regarding the optimization environment rather than the application, one of the latest trends in aircraft conceptual design optimization methods is the use of surrogate models. The basic methodology (see Forrester and Keane [11]) can be roughly summarized in a series of five steps: 1) selection of the variables to be optimized, 2) analysis of some initial sample designs, 3) generation of a model of the actual problem using a surrogate approach, 4) search in the design space for new design points of interest, 5) addition of new designs to those already available, and back (via iteration) to step 3. In the already referred review article by Forrester and Keane [11], the authors discussed various alternatives and explicitly stated that "since no method is truly universal, we give guidance as to each method's strengths and weaknesses." In particular, they described and discussed cross-validation, polynomials, moving least squares, radial basis functions, kriging, support vector regression, and enhanced modeling with additional design information. Another review on the same field was published a few years back by Queipo et al. [12]. In this article, apart from describing and discussing various techniques, the authors presented a practical case study consisting of the multi-objective design of a liquid-rocket injector. A different approach is the so-called collaborative optimization (CO) proposed initially by Kroo et al. [13]. The idea consists of decomposing the design problem into two levels: the system level whose responsibility is the coordination of the optimization process, and the lower level made up of subspaces for the various technical disciplines. The method has evolved along the years and has led to several improved versions such as those reported by Roth and Kroo [14] and Legresley and Alonso [15]. In this last version, the authors considered a high-fidelity aeroelastic design problem, in which the iterative process leading to the optimized solution is accelerated by means of improving the process of information exchange between the aerodynamics and structures computations. In particular, proper orthogonal decomposition (POD) modal description of the variables was used at the interfaces of the disciplines instead of the actual values of variables. For the sake of clarity, it is to be said that the algorithm being reported in the present article does not belong to the family of CO approaches. However, future coupling of CO and high-order singular value decomposition (HOSVD) may prove to be a suitable method to further increase the computational efficiency of the optimization process.

Finally, regarding the mathematical structure of the optimization algorithm, much effort has been devoted to the development and use of gradientlike methods in aircraft conceptual design related activities. Comprehensive reviews of these techniques can be found in, e.g., Chacksfield [16] and Jameson [17]. In parallel, it was soon recognized that other types of approaches were also well suited to the multidisciplinary nature of aerospace design. Back in 2002, Hajela [18] published a review on artificial neural networks, fuzzy logic-based function approximations, and evolutionary search and genetic algorithms for aerospace design applications. A recent similar review presenting later developments and a wider spectrum of approaches has been published by Lian et al. [19].

In this article, we present an optimization method for conceptual design in aeronautics applications that is based on the use of HOSVD. In particular, we have a higher system level for global optimization, based on a GA, and a lower level with subspaces for the technical disciplines based on HOSVD. The main difference with other methods is that before the start of the optimization process, we fill in some multiparametric databases with a limited number of computations (snapshots) from the technical disciplines. Then, we use these databases to generate surrogates of the technical disciplines that consist of HOSVD modal representation of the databases plus a quite efficient interpolation. Such surrogates allow for the fast calculation of the fitness of the individuals that come up during the GA evolution process. In other words, we perform the optimization not on the actual parametric space but on the HOSVD representation of this space. Regarding the organization of the article, some remarks on the computational needs and constrains of conceptual design are made in next section. After that, the methodology is first presented and then illustrated addressing the specific case study of the conceptual design of an unconventional empennage. Next, the results are evaluated and compared with those obtained by standard approaches and, finally, conclusions and some guidelines are provided. For the sake of clarity, details of the technical disciplines are relegated to the Appendix at the end of the article.

II. Remarks on Conceptual Design

Conceptual design has a large impact in the aeronautics industry. The reason is that even though, in theory, it should only aim to address the highest level questions about the proposed aircraft, in practice it tends to strongly influence decisions being made downstream during the design process. The whole structure of this design process has been described in detail by Price et al. [1]. In particular, they consider four phases: 1) conceptual design, 2) preliminary design, 3) detail design, and 4) general engineering design. The reason for this large impact of the conceptual design phase is that, usually, the whole process is tightly constrained by time and cost, meaning that the penalty associated with going backwards to rebate an earlier decision might not be assumed by the project management. In principle, the outcome of a conceptual phase, quoting Price et al. [1] literally, should be "a configuration with the basic size and arrangement of its main aspects such as the wing, empennage, engines, fuselages, control surfaces, etc."

In this context, conceptual design should aim to explore a very broad scope of many different configurations within a limited time constrain. The need to explore simultaneously distant regions of the parameter space has been pointed out by Antoine and Kroo [3] in their development of a framework for aircraft conceptual design. Also, in the introduction chapter of their article, Berard and Isikveren [20] state the following: "The conceptual design phase is typified by

the sizing of a multitude of design candidates generated by the need to construct a voluminous array of technical feasibility or trade studies under the limits of compressed timelines. This means that simple prediction tools must demonstrate characteristics of conformity, robustness, consistency, and applicability for the design problem at hand, with emphasis being placed upon an appropriate functional sensitivity to the free design variables." These statements also suggest the important fact that, in principle, fidelity of the tools used in this conceptual design phase should be low. For example, Price et al. [1] recommend the use of a few initial equations and empirical data, and Berard and Isikveren [20] propose the use of semi-empirical constructs. However, the main problem in dealing with unconventional configurations is that these empirical data/semi-empirical formulae for aerodynamic loads may not exist. This fact has been highlighted by Werner–Westphal et al. [10] when they write: "For unconventional aircraft configurations, empirical models are usually not available. The combination of higher fidelity models (more physics) and multidisciplinary design tools (more complexity) becomes necessary."

Summarizing, a tool for the conceptual design of unconventional configurations should:

1) Be able to explore a parameter space containing a very large number of potential candidates that, most likely, will differ widely from one another.

2) Be robust, consistent, and malleable. In other words, it should be such that different submodules can be integrated and interexchanged.

3) Be able to work with prediction tools that go one step beyond the standard semi-empirical constructs, which might be unavailable. And this should be done without steeping into the preliminary design phase, where higher fidelity models should be used.

In our opinion, the exploration of the whole parameter space is well served by the selection of a GA based search approach. Robustness and consistency are inherent in the HOSVD description of a multiparameter database. And the combination of the GA with the HOSVD description is computationally inexpensive enough as to allow for considering aerodynamic tools (such as aerodynamics vortex lattice (AVL) that, without being high-fidelity, are a more complex and reliable tool than semi-empirical constructs.

III. Description of the Method: High-Order Singular Value Decomposition Plus Interpolation (HOSVD + I)

The object of this section is to provide a general method for constructing surrogates of each technical discipline (e.g., aerodynamics), whose outcome can be seen as a scalar function of some design parameters and/or physical variables. Namely, the scalar outcome is given by

$$q = f(\mu^1, \ldots, \mu^n) \tag{1}$$

For example, the state variable q can be either the total lift of a wing depending on n design parameters, $\mu^1, \ldots, \mu^n$, or the overall chordwise lift, depending on $n-1$ design parameters, $\mu^1, \ldots, \mu^{n-1}$, and the position along the span μ^n. Discretizing the design parameters and/or physical variables in a structured manner, namely considering all combinations of $\mu^1, \ldots, \mu^n$, such that $\mu^k = \mu_1^k, \ldots, \mu_{N_k}^k$, we can construct the following n-th order tensor from the function (1)

$$A_{i_1 \ldots i_n} = f(\mu_{i_1}^1, \ldots, \mu_{i_n}^n) \tag{2}$$

This tensor builds an n-dimensional database, whose elements could be obtained using either wind-tunnel tests or computational fluid dynamics (CFD). According to our comments in Sec. III, in the application to conceptual design CFD will be based on an AVL method. The size of the database can be huge (especially if a large number of design parameters/physical variables is present), which can pose difficulties in manipulating the resulting data (to, e.g., calculating loads). Thus, a safe compression of such data is advisable. Multidimensional interpolation is also necessary to obtain the output q for intermediate values of the design parameters/physical variables.

Both tasks, namely controlled compression and interpolation are efficiently performed using HOSVD, which is explained now.

A. High-Order Singular Value Decomposition

To avoid a too involved notation, HOSVD is described for a generic third-order tensor; the extension to higher-order tensors is straightforward. The HOSVD of a $(N_1 \times N_2 \times N_3)$ tensor is of the form

$$A_{ijk} = \sum_{p,q,r} \sigma_{pqr} U_i^p V_j^q W_k^r \tag{3}$$

where the new tensor σ_{pqr} is known as the reduced tensor and the three vector families $\{U_i^1, \ldots, U_i^{N_1}\}$, $\{V_i^1, \ldots, V_i^{N_2}\}$ and $\{W_i^1, \ldots, W_i^{N_3}\}$ are known as modes of the decomposition.

The HOSVD can be seen as an extension to tensors of classical singular value decomposition (SVD), which only applies to matrices, but such extension is not a straightforward one. Let us recall here that the SVD of a matrix A_{ij} is [21] $A_{ij} = \sum \sigma_p U_i^p V_j^p$. Its most direct extension to tensors would be such that the coefficients of the modes depend only on one index, namely [cf, Eq. (3)] $A_{ijk} = \sum \sigma_p U_i^p V_j^p W_k^p$, but calculating such decomposition with a minimum number of terms is an ill-posed problem [22], except for some quite particular types of third-order tensors (e.g., tensors of order $2 \times N \times N$). And even defining such minimum number (known as the rank of the tensor) is an open problem nowadays [23]. The decomposition (3) is called a Tucker decomposition [24], and can be performed in a computationally efficient manner provided that the reduced tensor and the modes are appropriately defined. HOSVD is a Tucker decomposition in which modes are defined as the (orthonormal) eigenvectors associated with the positive eigenvalues of the positive definite, symmetric matrices B^1, B^2 and B^3, defined as [25]

$$B_{il}^1 = \sum_{jk} A_{ijk} A_{ljk}, \qquad B_{jl}^2 = \sum_{ik} A_{ijk} A_{ilk}, \qquad B_{kl}^3 = \sum_{ij} A_{ijk} A_{ijl} \tag{4}$$

Namely, the HOSVD modes are given by

$$\begin{aligned} \sum_{l=1}^{N_1} B_{il}^1 U_i^p &= (\alpha_p)^2 U_i^p, \qquad p = 1, \ldots, N_1 \\ \sum_{l=1}^{N_2} B_{jl}^2 V_j^q &= (\beta_q)^2 V_j^q, \qquad q = 1, \ldots, N_2 \\ \sum_{l=1}^{N_3} B_{kl}^3 W_k^r &= (\gamma_r)^2 W_k^r, \qquad r = 1, \ldots, N_3 \end{aligned} \tag{5}$$

where the positive scalars α_p, β_q, and γ_r will be referred to as the high-order singular values (HOSVs) of the decomposition. Once the HOSVD modes have been calculated, the reduced tensor σ_{pqr} is readily obtained multiplying Eq. (3) by the i, j, and k components of the HOSVD modes, adding in the indexes i, j, and k, and recalling that HOSVD modes are orthonormal. It follows that

$$\sigma_{pqr} \sum_{i=1}^{N_1} \sum_{j=1}^{N_2} \sum_{k=1}^{N_3} A_{ijk} U_i^p V_j^q W_k^r \tag{6}$$

Substitution of this into Eq. (3) provides an exact representation of the tensor A. However, if the elements of A show redundancies along the three dimensions (which can be due to, e.g., physical laws), then appropriate truncation of the expansion (3) still provides a good approximation. In fact, if the three sets of HOSVDs [namely, the eigenvalues of Eq. (5)] are sorted in a decreasing order and the decomposition (3) is truncated to $S_1 < N_1$, $S_2 < N_2$, and $S_3 < N_3$ terms, as

$$A_{ijk} \approx \sum_{p=1}^{S_1}\sum_{q=1}^{S_2}\sum_{r=1}^{S_3}\sigma_{pqr}U_i^p V_j^q W_k^r \tag{7}$$

Then the relative rms error of the truncated reconstruction of A is bounded by the following a priori relative error bound (see [25])

$$\text{APREB} \le \sqrt{\frac{\sum_{p=S_1+1}^{N_1}(\alpha_p)^2 + \sum_{q=S_2+1}^{N_2}(\beta_q)^2 + \sum_{r=S_3+1}^{N_3}(\gamma_r)^2}{\sum_{p=1}^{N_1}(\alpha_p)^2 + \sum_{q=1}^{N_2}(\beta_q)^2 + \sum_{r=1}^{N_3}(\gamma_r)^2}} \tag{8}$$

which allows for estimating the error before calculating the decomposition. Thus, truncated HOSVD allows for storing an approximation of the $N_1 \times N_2 \times N_3$ elements of the tensor A by means of only the $S_1 \times S_2 \times S_3 + S_1 \times N_1 + S_2 \times N_2 + S_3 \times N_3$ numbers involved in the right hand side of Eq. (7). This allows for a strong memory saving (and a potential decrease of the CPU time required to manipulate the elements of the tensor) when S_m is small compared with N_m. In other words, the compression factor scales with $S_1 \times S_2 \times S_3 / N_1 \times N_2 \times N_3$, which means that compression increases exponentially as the dimension of the tensor increases [26]. This emphasizes the fact that because of redundancies, the relevant information in a database is much smaller than its size, and that the ratio between both can be quite small if all redundancies along all dimensions in the database are appropriately taken advantage of (as done when using HOSVD).

Summarizing, the HOSVD modes and singular values are calculated from the eigenvalue problems (5), with the coefficient matrices B^1, B^2, and B^3 as given in Eq. (4). The a priori error estimate in Eq. (8) allows for truncating the decomposition (7) to meet error requirements. Finally, the core tensor is calculated using Eq. (6).

Some care must be taken to optimize the computational cost of the process:

1) Eq. (4) may involve a huge number of operations, especially in higher dimensional tensors. To control this in the calculation of, e.g., B^1, (when $N_2 \times N_3$ is large compared with N_1), the second and third indexes of the tensor A are sorted together to obtain a matrix $\tilde{A}$, with N_1 rows and $N_2 \times N_3$ columns, which is such that $B^1 = \tilde{A}^T\tilde{A}$. Application of a QR decomposition to such matrix yields $\tilde{A}E = QR$, where E is a column permutation orthogonal matrix, Q is an orthogonal matrix, and R is an upper triangular matrix. Thus, B^1 is calculated as $B^1 = \tilde{A}^T\tilde{A} = ER^TQ^TQRE^T = ER^TRE^T$, which involves much fewer operations than those required in Eq. (4).

2) Appropriate factoring of the right hand sides of Eqs. (6) and (7) (to avoid repeating calculations) greatly improves computational efficiency.

Now, with the above HOSVD decomposition we can construct a compressed model of the database that results from discretizing the function (1). Considering, as above, the case $n = 3$, the HOSVD representation is of the form

$$f(\mu_i^1, \mu_j^2, \mu_k^3) = A_{ijk} \approx \sum_{p=1}^{S_1}\sum_{q=1}^{S_2}\sum_{r=1}^{S_3}\sigma_{pqr}U_i^p V_j^q W_k^r \tag{9}$$

B. Multidimensional Interpolation

Equation (9) provides the values of the function f at the discretized values of the independent variables. Such representation can also be seen as

$$f(\mu^1, \mu^2, \mu^3) \approx \sum_{p=1}^{S_1}\sum_{q=1}^{S_2}\sum_{r=1}^{S_3}\sigma_{pqr}u^p(\mu^1)v^q(\mu^2)w^r(\mu^3) \tag{10}$$

where the functions u^p, v^q, and w^r are defined in terms of the HOSVD modes as

$$u^p(\mu_i^1) = U_i^p, \qquad v^q(\mu_j^2) = V_j^q, \qquad w^r(\mu_k^3) = W_k^r \tag{11}$$

The values of these three functions at other, intermediate values of μ_1, μ_2, and μ_3 are readily obtained by (e.g., spline) interpolation. Thus, HOSVD allows for reducing the three-dimensional interpolation that would be needed in principle to three one-dimensional interpolations, which are easier and much more computationally efficient. This method to obtain surrogates of technical disciplines will be referred to as HOSVD + I below.

C. Genetic Algorithm Formulation

The optimization method is a GA, which is chosen to be both simple and robust: 300 individuals per generation are considered, and a total number of 500 generations are run unless convergence occurs sooner. The cross over and mutation probabilities at bit level have been set to 90 and 4%, respectively. Additionally, an elite subpopulation of 10% of the total population is made to pass unchanged to the next generation. Additional information regarding the details of the GA can be found in the article by Alonso et al. [27]. Nevertheless, this formulation can be certainly improved, most probably combined with a gradientlike method such as steepest descent, so as to generate a hybrid optimization method that runs significantly faster than the one used in this article.

IV. Case Study

The methodology presented above is now illustrated with a specific case study: the problem of optimizing a commercial aircraft empennage according to a prescribed multidisciplinary objective function and a set of restrictions. The HOSVD + I method is applied to obtain surrogates of the various technical disciplines, which are much more computationally efficient than the original models. It is to be said that this is a fairly simplified exercise on conceptual design. The number of free parameters has been kept small enough, in such a way that the complete set of calculations, including computations of snapshots, can be run in a standard PC. In addition, our selection of hypotheses, ingredients of the objective function, and set of restrictions is rather simplified and debatable; and aeroelastic restrictions are not considered. Thus, we do not claim that the outcomes are configurations to be considered as actual candidates for future aircraft. Instead, what we intend is to illustrate and discuss here the practical implementation of our methodology, its advantages and drawbacks, and its potential as a tool to make quick trade-offs during the early phases of the design cycle.

Let us now anticipate the main ingredients of the optimization method. A detailed description is provided in the Appendix at the end of the paper.

A. Objective Function

Starting from a given reference empennage configuration to be specified below, the aim is to minimize the following objective function, which contains three terms related to three different criteria, namely the weight of the structure, the viscous drag, and the geometrical complexity (which is somewhat related to cost):

$$\Phi = \varepsilon_1 \frac{\text{weight}}{\text{weight}_{\text{ref}}} + \varepsilon_2 \frac{\text{drag}}{\text{drag}_{\text{ref}}} + \varepsilon_3 \frac{\text{complexity}}{\text{complexity}_{\text{ref}}} \tag{12}$$

where the subscript ref denotes the reference configuration, and ε_1, ε_2, and ε_3 are weight factors that are selected such that $\varepsilon_1 + \varepsilon_2 + \varepsilon_3 = 1$. The three ingredients above will be calculated using surrogates, as explained in Appendices A.I.B, A.I.C, and A.III.B.

In particular, the surrogate for weight (which will be the most computationally expensive ingredient) will be based on various lower order surrogates for the aerodynamic loads, constructed in the Appendix A.III.A from aerodynamics calculations based on AVL. The loads that dimension the structure are computed at the following flight conditions: altitude $= 1,500$ m, and Mach $= 0.5$. The horizontal tail plane (HTP) is dimensioned with the most critical among the following values of the angle of attack and sideslip angle, namely $(\alpha, \beta) = (0°, 10°)$, (10°,0°), and (5°,5°); the vertical tail plane (VTP) is sized at the less favorable conditions among the above

mentioned, which is $(\alpha, \beta) = (0°, 10°)$. Viscous drag is calculated with a simple wetted area model at cruise conditions: altitude= 1500 m, Mach = 0.8, and $\alpha = \beta = 0°$. Complexity is evaluated from purely geometrical properties.

A rigorous approach to find the Pareto optimal solutions of the multi-objective optimization process described by Eq. (12) would require the use of a methodology (based on multi-objective genetic algorithms, or MOGAs) of the type described by Eddy and Lewis [28] and Ferguson et al. [29]. For the sake of simplicity, the simpler GA method described in Sec. IV.C will be used, although a possible future area of research would be to explore the combination of MOGAs and HOSVD.

B. Restrictions

The search for the optimum configuration is subject to the following restrictions, which are calculated at altitude = 1500 m, and Mach = 0.2:

1) R1: The conveniently scaled (see Appendix A.II.A) stability derivatives of the empennage with respect the angle of attack and the sideslip angle, $C_{m\alpha}$ and $C_{n\beta}$ are not allowed to worse their counterparts in the reference configuration, which are $C^{\text{ref}}_{m\alpha} = -2.8\ \text{deg}^{-1}$ and $C^{\text{ref}}_{n\beta} = 0.13\ \text{deg}^{-1}$, respectively.

2) R2: Similarly, the vertical and horizontal control derivatives with respect to the horizontal and vertical control surfaces deflection angle (both denoted as δ), $C_{m\delta}$, and $C_{n\delta}$, are required to be at least a 90% of their counterparts in the reference configuration, which are $C^{\text{ref}}_{m\delta} = -1.24\ \text{deg}^{-1}$ and $C^{\text{ref}}_{n\delta} = 0.07\ \text{deg}^{-1}$, respectively.

3) R3: Stall is assumed to occur, and the individual is discarded, if either the maximum or minimum (along the span) values of the chordwise lift coefficient reach some threshold values, which are assumed to be $Cl^{\text{ref}}_{\text{max}} = 1.57$ and $Cl^{\text{ref}}_{\text{min}} = -1.57$, respectively.

Surrogates for the stability and control derivatives, and the maximum and minimum spanwise values of the lift coefficient are constructed in the Appendices A.II.A and A.II.B. The approach that has been actually followed has been to discard those individuals that do not meet either of the restrictions R1, R2, or R3. A possible reasonable alternative could have been to retain these individuals in the GA population and apply a penalty function to their fitness value modifying Eq. (12). The reason to choose the former criterion instead of the latter is that civil aircraft design and manufacturing tends to be a rather conservative activity and, normally, new concepts are accepted only if they improve previous ones both globally and, to some extent, locally. In this sense, aircraft handling and controllability are key technical issues and we decided to treat them as a series of clean cut restrictions.

C. Reference Configuration

The reference configuration (see the sketch in Fig. 1) is a highly simplified aircraft configuration characterized by the following parameters:

1) Fuselage (with a circular cross-section): maximum diameter = 8 m and length = 65 m.

2) Wing: profile = NACA4412, swept angle = 40°, dihedral angle = 5°, taper ratio = 0.2, and semispan = 30 m.

3) HTP: profile = NACA0012, root chord = 10 m, swept angle = 0°, dihedral angle = 0°, taper ratio = 0.5, and semispan= 15 m.

4) VTP: profile = NACA0012, root chord = 10 m, swept angle = 31°, taper ratio = 0.5, and semispan = 15 m.

D. Design Parameters

The fuselage and the wings are kept fixed in the optimization process. Each HTP consists of an internal trapezoidal piece and an external piece in which a quadratic correction of the dihedral deformation is also allowed; the VTP is trapezoidal. The empennage geometry is defined with the following nine parameters: 1) the lengths of two pieces of the HTP, λ_1, λ_2; 2) the HTP swept angle λ_3; 3) the dihedral angle of the HTP λ_4, and a quadratic correction in the external piece of the HTP λ_5; 4) the taper ratio of the HTP λ_6; 5) the total height of the VTP λ_7; 6) the swept angle of the VTP λ_8; and 7) the taper ratio of the VTP λ_9.

These parameters are allowed to vary in the following ranges: $7\ \text{m} \le \lambda_1 \le 22\ \text{m}$, $0 \le \lambda_2 \le 15\ \text{m}$, $-1 \le \lambda_3 \le 1$, $0 \le \lambda_4 \le 1$, $-1\ \text{m}^{-1} \le \lambda_5 \le 1\ \text{m}^{-1}$, $0.1 \le \lambda_6 \le 1$, $0 \le \lambda_7 \le 16\ \text{m}$, $-1 \le \lambda_8 \le 1$ and $0.1 \le \lambda_9 \le 1$.

With these ingredients (detailed in the Appendix), a reduced optimization tool, based on surrogates for the technical disciplines has been constructed with the HOSVD + Interpolation tool described in Secs. III.A and III.B. To this end, each parameter is discretized with a total number of six equispaced values. For each technical discipline, the AVL method is run for all combinations of the resulting discretized values of the parameters, to obtain the snapshots that will be used to calculate the HOSVD step of the HOSVD + Interpolation tool. Note that the maximum number of runs occurs in the HTP, which depends on six free parameters and thus requires 6^6 runs. The a priori relative error bound Eq. (8) for truncation of the HOSVD step is set to 1%; in addition, the maximum relative error in reconstructing all snapshots is calculated a posteriori and required to be smaller than 5%.

V. Results and Discussion

The performance of the reduced optimization tools is now analyzed. These have been run a total number of 36 times. Ten of them have been used to calibrate the complexity function, as explained in the Appendix A.I.B). The remaining 26 runs have been performed in two campaigns, considering seven and 12 combinations of the three weights appearing in the objective function (12), which are considered in Secs. V.A and V.B below.

A. First Optimization Campaign

Two sets of seven runs of the optimization tool have been performed for the seven combinations of the weights in the objective function (12) indicated in Table 1. The GA is run in a standard way for these combinations in the first seven runs. The resulting

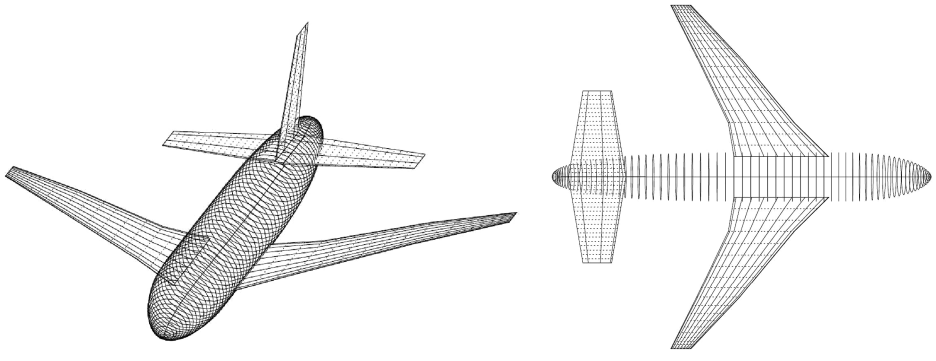

Fig. 1 Reference configuration.

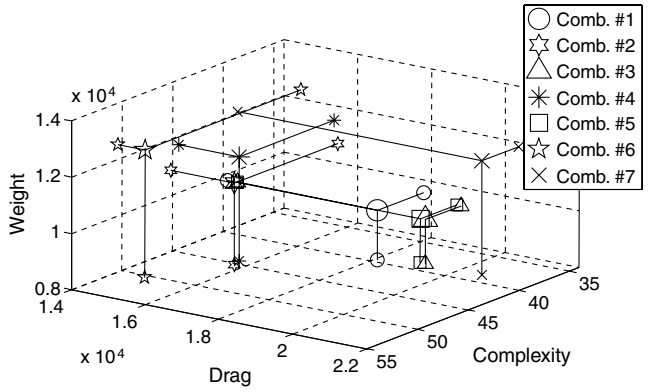

Fig. 2 Weight/drag/complexity for the optimized individuals in the first optimization campaign.

optimized individuals of the seven combinations are added as seeds in the subsequent seven combinations to ensure that new regions of the parameter space are considered in the GA runs. The values of the weight, drag, and complexity of the optimized individuals in the second run are also provided in Table 1, and illustrated in the diagram of Fig. 2, where their counterpart for the baseline configuration is also provided for reference. Note that:

1) The baseline drag and complexity is always improved, even in those combinations that do not take these into account. Weight is also improved except in combinations 4 and 6.

2) Weight and viscous drag show opposite trends, as do drag and complexity. This can be explained noting that increasing the span of the HTP decreases the wet area and thus viscous drag, but increases both the bending moment and the length of the generatrix, which in turn increases both weight and complexity.

3) Weight and complexity instead show the same trend, which is further appreciated in the fact that combinations 3 and 5 provide almost the same result.

4) Combinations 1–5 and 7 produce qualitatively similar optimized configurations, which are always *V*-shaped. They differ only in the quantitative values of the various parameters of the HTP, such as the swept and dihedral angles. The VTP is absent in all combinations. Thus, lateral stability and control are more efficiently accounted for through the dihedral angle of the HTP than with the additional inclusion of a VTP, which penalizes the three ingredients in the objective function.

5) Combination 6 promotes a quadratic correction of the dihedral angle, which decreases viscous drag (subject to the imposed restrictions), the only objective function ingredient that is present in this combination. Such quadratic complexity penalizes both weight and complexity, and thus is absent in the optimized individuals resulting from the remaining combinations.

Since the results in this section are discussed as a matter of illustration (not intending to provide actual empennage configurations), only configuration 1 will be considered below in some detail; the main difference with configuration 6 will also be illustrated. Both configurations 1 and 6 are illustrated in Fig. 3.

Table 2 shows the parameter values of the optimized individual in combination #1; note that the GA provides values for the HTP and the VTP parameters, but the height of the VTP is $\lambda_7 = 0$, meaning that the VTP is in fact absent. The actual values of the restrictions are also indicated for both the baseline and the optimized configurations, as well as the optimized values of the weight, drag, and complexity, and the fitness. Note that the optimized individual improves the baseline in the three ingredients of the objective function. The generatrices of the HTP and VTP in the empennage along the optimization process in combination 1 and 6 are sketched in Fig. 4, where the various generatrices are plotted. For reference, the baseline configuration is plotted with dashed lines. It is to be noted that the initial approach to the optimized configuration is quite fast. For instance, the vertical stabilizer has been eliminated in the ninth generation of the GA.

A further illustration of the optimization process in combination 1 is provided in Fig. 5, where the evolution of the taper ratio of the HTP and the fitness (global, as well as fitnesses for the three ingredients of the objective function) are provided; fitnesses of are plotted. Note that optimization is essentially completed at generation 50th.

B. Second Optimization Campaign

Now, the optimization tool is run for the 12 combinations presented in Table 3. As in the first campaign, the three ingredients of the objective function are improved in the optimized configurations, except for weight in combinations 2 and 4, which illustrates the

Table 1 The seven combinations considered in the first optimization campaign (columns 2–4) and the associated values of the weight, drag, complexity, and fitness of the optimized configurations (columns 5–7); the baseline weight/drag/complexity is also given for reference

	ε_1	ε_2	ε_3	Weight, kg	Drag, N	Complex.	Fitness
Comb. # 1	1/3	1/3	1/3	9759	18,070	39.6	0.84
Comb. # 2	1/2	1/2	0	10,836	15,734	45.2	0.90
Comb. # 3	1/2	0	1/2	9521	18,964	38.6	0.76
Comb. # 4	0	1/2	1/2	14,651	15,636	44.4	0.80
Comb. # 5	1	0	0	9511	19,025	38.7	0.85
Comb. # 6	0	1	0	12,205	15,016	49.7	0.79
Comb. # 7	0	0	1	9641	20,614	38.2	0.67
Reference	——	——	——	11,124	19,129	57.1	——

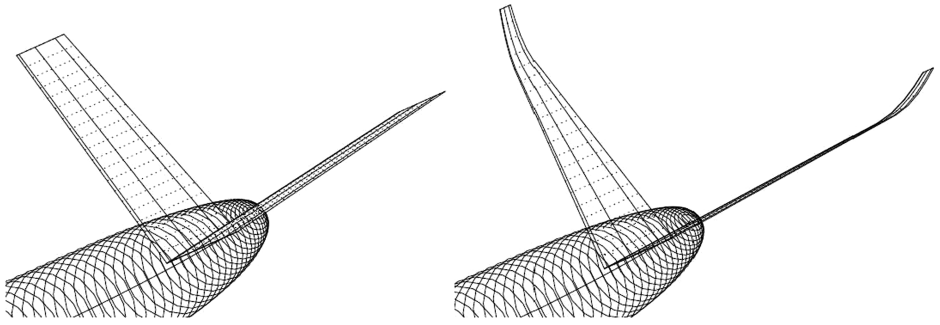

Fig. 3 Configurations 1 and 6.

Table 2 The optimized configuration in combination 1; the baseline configuration is also considered for reference

HTP parameters					VTP parameters			
λ_1	λ_2	λ_3	λ_4	λ_5	λ_6	λ_7	λ_8	λ_9
19.66	0.15	0.2598	0.7559	0.0236	0.6669	0.0	−0.3701	0.3055

Restriction	Baseline	Optimized configuration
C_{m_α}	−2.80	−2.81
C_{n_β}	0.13	0.13
C_{m_δ}	−1.24	−1.63
C_{n_δ}	0.071	0.133
$C_{l_{\max}}$	1.57	1.51
$C_{l_{\min}}$	−1.57	−1.24

Optimization function	Baseline	Optimized conf.	Fitness
Weight	11,124	9759	0.88
Drag	19,119	18,070	0.94
Complexity	57.0	39.6	0.69
Total fitness	1.00	0.84	

consistency of the results. For the sake of brevity, the remaining results are omitted; we just point out that the trends in the first campaign are confirmed here. In particular, all optimized configurations are *V*-shaped, either exhibiting only the internal flat piece or with a short external curved piece, but with a quite small quadratic correction, which gives a maximum correction of 1 cm in the vertical deflection of the HTP.

C. Reduced Optimization Tool vs Conventional Optimization Tool

Results obtained with the reduced optimization tool in the first optimization campaign, combination 1, are compared in Table 4 with its counterparts obtained with a conventional optimization tool (not using the surrogates for the various technical disciplines), based on the same GA. As can be seen, the relative error is always below 3%. Results for the remaining combinations in the first campaign and for all combinations in the second campaign are completely similar, except for the restriction on lateral stability, which shows larger errors (up to 7%) in some cases. The larger relative errors are associated with the fact that this restriction shows quite small values, and can be even due to round off errors in the AVL results. In any event, those errors could be decreased by both retaining more modes in the HOSVD (which also requires calculating a larger number of snapshots) and improving the precision of the AVL method (using a finer grid). This is out of the scope of the method performances illustration, which is the object of this section, and will not be pursued any further here.

Concerning reduction of the required computational time, which is what has been pursued with the reduced optimization tool, calculation of the properties of each configuration requires 0.0037 CPU seconds with the reduced tool, and 9.7 CPU seconds with the conventional tool that uses AVL to calculate the aerodynamics of each individual. Thus, if the GA optimization algorithm involves 300 individuals per generation and 500 generations, each optimization run requires 1.56 CPU hours using the reduced tool and 405.4 CPU hours using the conventional optimization tool, which means that the computational effort has is divided by a factor of 260 if only the optimization runs are considered. The reduced tool requires the previous AVL-calculation of the snapshots that are needed to

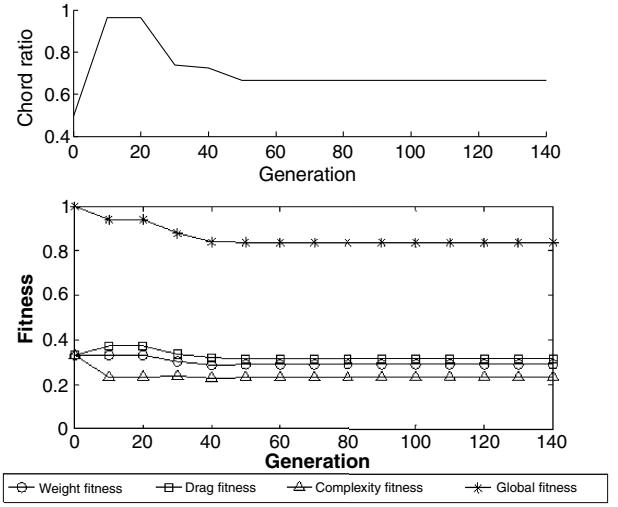

Fig. 5 a) HTP chord ratio evolution along the optimization with combination 1, and b) evolution of the optimization function.

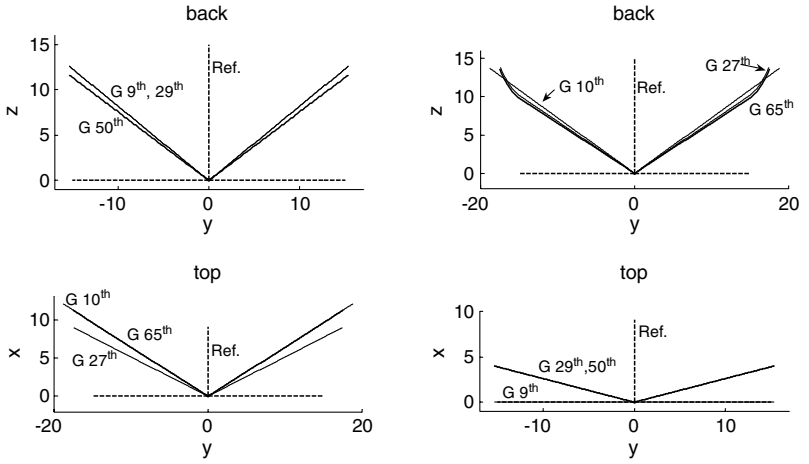

Fig. 4 Top and back views of the evolution of the generatrices along the optimization run for combinations 1 (left) and 6 (right). The reference configuration is plotted with dashed lines. Distances are in meters.

Table 3 Counterpart of Table 1 for the 12 combinations in the second optimization campaign

	ε_1	ε_2	ε_3	Weight, kg	Drag, N	Complex.	Fitness
Comb. # 1	0	1/3	2/3	10,510	17,937	39.5	0.77
Comb. # 2	0	2/3	1/3	15,181	15,223	46.2	0.80
Comb. # 3	1/3	0	2/3	9520	18,963	38.6	0.73
Comb. # 4	1/3	2/3	0	11,158	15,426	46.7	0.87
Comb. # 5	2/3	1/3	0	9713	18,064	39.6	0.89
Comb. # 6	2/3	0	1/3	9520	18,963	38.6	0.79
Comb. # 7	1/6	1/6	2/3	9520	18,963	38.6	0.76
Comb. # 8	1/6	2/3	1/6	11,149	15,436	46.7	0.84
Comb. # 9	2/3	1/6	1/6	9520	18,963	38.6	0.85
Comb. # 10	1/4	1/4	1/2	9520	18,963	38.6	0.80
Comb. # 11	1/4	1/2	1/4	10,376	16,377	42.7	0.85
Comb. # 12	1/2	1/4	1/4	9520	18,963	38.6	0.84
Reference	——	——	——	11,124	19,129	57.1	——

Table 4 Comparison between the full and reduced optimization tools in combination 1, first optimization campaign

Restriction	Reduced tool	Full tool	Error
C_{m_α}	−2.81	−2.84	1.1%
C_{n_β}	0.13	0.13	0.0%
C_{m_δ}	−1.63	−1.68	3.1%
C_{n_δ}	0.133	0.135	1.5%
$C_{l_{\max}}$	1.51	1.55	2.6%
$C_{l_{\min}}$	−1.24	−1.21	2.5%
Optimization function	Reduced tool	Full tool	Error
Weight	9759	10,052	3.0%
Drag	18,070	18,070	0.0%
Complexity	39.6	39.6	0.0%
Total fitness	2.51	2.53	0.8%

generate the surrogates, which involve the following computational effort: 1) stability and control: 17 CPU hours, 2) aerodynamics loads: 52.7 CPU hours, and 3) stall calculations: 52.7 CPU hours.

If these 122.5 CPU hours are added to the optimization computational effort, the resulting CPU time is 124.1 hours, which means that the CPU time required by the conventional optimization tool to perform one optimization run (405.4 hours) has been decreased by a factor of 3.6 in just the first optimization run. But, as it happened in the illustration above, conceptual optimization usually requires a large number of additional optimization runs associated with both calibration and reformulation of the underlying assumptions (depending on intermediate results), which do not require recalculating the surrogates if flight conditions remain unchanged. As the number of additional optimizations increases, the benefit of the reduced model increases, approaching the asymptotic reduction factor of 260. For instance, in the 36 optimization runs performed in Secs. V.A and V.B above, the reduction factor was $36 \times 405.4/(122.5 + 36 \times 1.56) = 81.7$. It is also to be noted that the CPU time required by the conventional computational tool (608 CPU days) would make this tool impractical in this task, while its counterpart for the reduced tool (7 days) is quite reasonable.

Note that all CPU times mentioned above scale with the number of AVL runs that are necessary using either the conventional tool and the reduced tool developed in above. Thus, the saving factors 3.6 and 260 mentioned above are independent of the fidelity of the CFD solver. In other words, the reduced tool would show the same advantages if a high-fidelity CFD solver (such as a Reynolds-averaged Navier–Stokes solver) were used. The problem would be the huge amount on CFD runs that would be necessary (using either the conventional and the reduced tool), which is ultimately the reason for not using high-fidelity models in conceptual design, as explained in Sec. III.

D. Further Improvements of the Method

As developed above, the reduced optimization tool meets all requirements enumerated in Sec. III above. In particular, it provides results comparable to the full optimization tool in a much smaller computational time, since the CPU time required to generate the surrogates was 3.6 times smaller than that required by the full optimization tool to perform one single optimization run. After that, each optimization run with the reduced model requires a CPU time that is 300 times smaller than that required by the conventional tool. Thus, the main advantage of the reduced tool is clearly illustrated. Further improvements, which are beyond the scope of this paper, could result in reducing the preprocess (to construct the surrogates) computational time, which required 6^6 runs of the aerodynamic solver in a structured mesh in the parameter subspace associated with the HTP geometry (the VTP geometry depended on a fewer number of parameters). A large reduction of the preprocess CPU time could result from the following observations:

1) The geometrical constrains (which can be imposed a priori) are met by only 36.8% of the 6^6 considered configurations; such reduction would exponentially increase when the number of design parameters is increased. Thus, considering only those configurations than meet the geometrical constrains reduces the computational effort, but requires considering nonstructured meshes, which in turn requires to appropriately modify the HOSVD description. Such extension of HOSVD is the object of our current research.

2) Aerodynamic/aeroelastic/control constrains are met by only a 5.8% (this percentage decreases to 5.5% if geometrical constrains are also considered) of the 6^6 configurations, which would lead to a stronger CPU time reduction; again, such reduction would exponentially increase when the number of design parameters is increased. These constrains are not known a priori, but could be either: 1) estimated using a lower fidelity aerodynamic solver/empirical construct, or 2) imposed sequentially when constructing the surrogates for the various technical disciplines (namely, those configurations that do not meet the constrain associated with the surrogate for a the technical disciplines are not considered when constructing the surrogates for the remaining technical disciplines). Again, considering only those configurations that meet all constrains requires the modification of the HOSVD description.

3) Constructing the HOSVD tool should not require computing all points of the structured mesh in the parameter space, but only the much smaller subset that is associated with compressed description provided by the HOSVD decomposition, which requires an appropriate selection of the configurations that are actually calculated. It is to be noted here that the compression factor increases exponentially as the dimension of the database increases [26]. The difficulty is of course to identify those points of the parameter space that should be calculated by the aerodynamic solver to obtain optimal results. This is related to the so-called sampling problem, and is currently the subject of active research, see [30,31], and references therein.

The necessity of reducing the preprocess CPU time associated with POD/SVD based model reduction methods is an ubiquitous problem, whose solution would be of interest in many applications of these methods, and is the object of our current research. But this is also well beyond the object of the present article and will not be pursued here any further.

VI. Conclusions

A method has been presented for conceptual design in aeronautics that is made up of two levels. A GA is in charge of optimizing a target function that accounts for various multidisciplinary ingredients (e.g., weight, drag, and geometrical complexity). The various technical disciplines are modeled using surrogates (at various sublevels) that are constructed using a combination of HOSVD and one-dimensional interpolation. The computation of the surrogates requires running the original computational tools (for, e.g., aerodynamics) at some structured, discretized values of some subsets of the set of free design parameters. In fact, for each technical discipline, the computational tool must be run only for the free parameters involved in the discipline, which is always smaller than the total number of free parameters. Thus, the advantages of the reduced model become more evident as the number of free parameters increases. For instance, if quadratic corrections are added to the swept angles of the HTP and the VTP and a linear torsion of the HTP is considered, and four free parameters (two for the HTPs and two for the VTP) were added, then seven additional parameters must be added. This significantly increases (from 9 to 16) the dimension of the search space. With a conventional tool, this requires the GA to exponentially increase the number of individuals per generation. With the reduced model instead, the number of geometrical free parameters in the HTP and the VTP is increased from six to eight and from three to four, respectively, which involves an affordable increase in the computational effort associated with constructing the aerodynamics surrogates; a surrogate could be constructed for the structure (to account for the new structural free parameters) whose calculation would be quite inexpensive. All these involve a much lower increase in the required than that associated with the conventional tool.

The surrogates are much more computationally efficient than the conventional computational tool (namely, the required CPU time was decreased by a factor of 81.7 in the example considered above) and can be defined as independent of the various modeling parameters that must be tuned in advance. Thus, tuning as well as optimization can be performed using the surrogate models. This makes the advantages of the reduced model even more evident. For instance, in the example considered in the article, the number of free design parameters was nine and five additional tunable parameters (the three weights in the objective function and the parameters b and m appearing in the definition of complexity) were present. For simplicity, no additional tunable parameters (e.g., the various safety factors and other parameters appearing in the structure calculation) were considered. The number of tunable parameters in actual conceptual design can be quite large, which could make it impractical to tune the various parameters in the method using the conventional optimization tool; with the surrogates instead, the computational cost of tuning can be reasonable, even in a standard PC.

In fact, CPU time is a quite important issue in conceptual design, which must be performed within specific cost and time constrains. Therefore, an optimization method cannot be accepted unless those constrains are met, irrespective of how robust, flexible, and reliable the method can be. In such a scenario, it is expected that the method presented in this article, which is flexible enough to be combined with any specific optimization method, is a promising alternative to current approaches.

For the sake of brevity, the illustration of the method in Sec. V was rather simplified, but the advantages of the method would be even clearer in more realistic conceptual design problem, which could include:

1) More free parameters in the definition of the HTPs and the VTP, to account for, e.g., torsion in the HTP and higher-order corrections in the various polynomial approximations.

2) A more detailed model of the structure.

3) A better modelization of viscous drag and stall, using a more detailed description of the boundary layer.

The method developed in the article was a basic version, which could be improved in various ways:

1) A multifidelity approach could be used, in which various aerodynamic models (based on, e.g., a panel method or a finite volume + turbulence model method) are sequentially used, in the whole parameter spaces and in subregions near preoptimized configurations.

2) A multi-objective GA would give a better performances than the more standard GA that has been used.

3) The computational effort required to construct the surrogates for the various technical disciplines can be reduced strongly, as explained in Sec. IV.D.

4) A gradientlike method can be combined with the GA to speed up convergence of the elite individuals.

Appendix: Description of the Technical Disciplines and the Surrogates

I. Purely Geometrical Ingredients

After defining the parameterizations of the HTP and the VTP, we describe the two ingredients of the target function that only depend on the geometry, namely, the geometrical complexity and the viscous drag.

A. *Parametrization of the Geometry*

The HTP consists of two pieces (sketched in Fig. A1), which are smoothly assembled. The internal piece is flat and trapezoidal but a quadratic correction of the dihedral angle is also included in the external piece. Each HTP is described using a generatrix that provides the centers of the chordwise sections and is given by

$$x = \lambda_3 y \quad \text{if } y > 0 \qquad z = \lambda_4 y \quad \text{if } 0 < y < \lambda_1/\sqrt{1+\lambda_3^2+\lambda_4^2}$$
$$z = \lambda_4 y + \lambda_5 (y - y_1)^2 \quad \text{if } y > \lambda_1/\sqrt{1+\lambda_3^2+\lambda_4^2} \tag{A1}$$

in terms of the Cartesian coordinates x, y, and z, with origin at the center of the root section, the x axis along the fuselage axis, the z axis contained in the plane of the root section pointing upwards, and the y axis perpendicular to the fuselage symmetry plane pointing to the right. Thus, the generatrix consists of a straight segment whose length is λ_1, followed by a parabolic segment, whose length is λ_2. Imposing the latter requirement requires solving the equation $s(y) - s(y_1) = \lambda_2$, where $y_1 = \lambda_1/\sqrt{1+\lambda_3^2+\lambda_4^2}$ and the arch length along the generatrix is defined in terms of the spanwise coordinate as

$$s = \int_0^y \sqrt{1+\lambda_3^2+z'(y)^2}\,\mathrm{d}y$$

Thus, the HTP is defined in terms of six free parameters: $\lambda_1 \geq 0$, $\lambda_2 \geq 0$, λ_3 (proportional to the tangent of the swept angle), λ_4 (proportional to the tangent of the dihedral angle), λ_5 (quadratic correction to the dihedral angle), and λ_6 (the taper ratio).

The chordwise section is a NACA0012 airfoil profile, whose center moves along the generatrix in such a way that its mid line is always parallel to the x axis and the airfoil is always contained in the normal plane of the projection of the generatrix on the $y-z$ plane (see Fig. A1, left plots). In other words, the angle between the airfoil plane and the $x-z$ plane is such that

$$\sin\theta = z'(y)/\sqrt{1+z'(y)^2} \tag{A2}$$

The (ruled) surface generated by the mid lines of the 2-D airfoils will be called the midlines surface below. Both the chord and thickness of the 2-D airfoil vary with the same linear law along the whole HTP, namely

$$c = c_r + \frac{\lambda_6 - 1}{\lambda_1 + \lambda_2} c_r s(y) \tag{A3}$$

where c_r is the chord at the root section and $\lambda_6 > 0$ is the taper ratio.

The VTP (see Fig. A1, right plots) is trapezoidal, with a planform homothetic to that of the baseline HTP. The cross section is the same as that of the HTP (NACA0012). Thus the VTP shape depends only

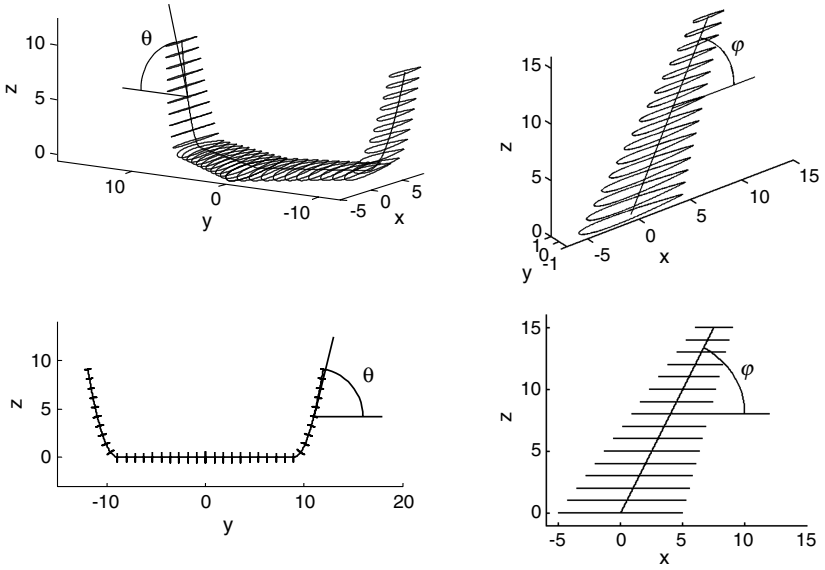

Fig. A1 Generation of the HTP (left) and the VTP (right).

on three parameters, namely the height λ_7, the swept λ_8, and the taper ratio λ_9.

Two examples of the resulting empennage configurations are those optimized configurations obtained in Sec. V (see Fig. 3). Two additional examples are provided in Fig. A2.

B. Geometrical Complexity

Using the parametrization defined above, the geometrical complexity of the empennage is calculated adding the contributions from the HTP and the VTP, as

$$C_{\text{EMPENNAGE}} = (1+b)(2C_{\text{HTP}} + C_{\text{VTP}})$$

where the penalty b is applied when a VTP is present. The complexity of the HTP is estimated as

$$C_{\text{HTP}} = \int_0^{\lambda_1+\lambda_2} \sqrt[m]{1+\left|\kappa(s)\right|^m}\,\mathrm{d}s \tag{A4}$$

where s is the arch length along the generatrix as above and κ is the curvature of the generatrix. Since the generatrix of the VTP is a straight line, it exhibits zero curvature and the complexity of the VTP is defined as

$$C_{\text{VTP}} = \int_0^{\lambda_7\sqrt{1+\lambda_8^2}} \sqrt[m]{1+\left|\kappa(s)\right|^m}\,\mathrm{d}s = \lambda_7\sqrt{1+\lambda_8^2} \tag{A5}$$

where λ_7 is the HTP height and λ_8 is proportional to the tangent of the swept angle.

The exponent m and the penalty b are to be calibrated, noting that increasing m emphasizes the effect of high concentrated values of κ, which occur in, e.g., sharp junctions between smooth pieces of the HTP. After some calibration that consisted in a campaign of GA runs (for various values of m and b) similar to the campaigns described in Sec. V, the following values have been selected

$$b = 0.1, \qquad m = 2 \tag{A6}$$

Since calculation of the integrals (A4) and (A5) is computationally inexpensive, no surrogate model is constructed to calculate complexity.

C. Viscous Drag

The total viscous drag is calculated at cruise conditions (altitude = 15,000 m, Mach = 0.8) using a flat plate boundary-layer analogy, which allows for adding the contributions of the HTPs and the VTP

$$D = 2D_{\text{HTP}} + D_{\text{VTP}}$$

The contribution from each HTP (the VTP is treated similarly) is given by

$$D_{\text{HTP}} = \frac{1}{2}c_f\rho_\infty U_\infty^2 W_A \tag{A7}$$

where ρ_∞ and U_∞ are the density and velocity at the freestream, W_A is the wetted area of the HTP, and c_f is the friction coefficient. The latter is estimated as [32]

$$c_f = 0.455/(\log Re_m)^{2.588} \tag{A8}$$

where Re_m is the Reynolds number, based on the HTP mean chord.

As it happened with complexity, these calculations are computationally inexpensive and thus no surrogate model is constructed.

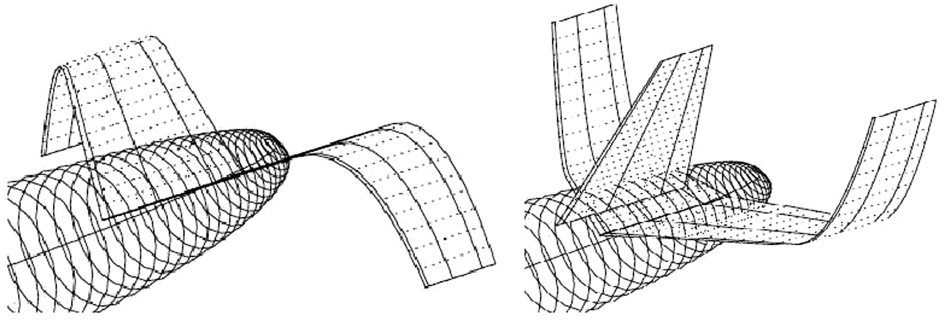

Fig. A2 Two examples of empennages generated with the parametrization described above.

II. Aerodynamic Restrictions

Aerodynamic restrictions involve the lift coefficient and the stability and control derivatives of the empennage. Aerodynamic interaction between the HTP and VTP is neglected. Thus both the total lift coefficient and the stability and control derivatives of the empennage are calculated adding the contributions of the HTP and VTP, which are calculated using the AVL method to the fuselage/wings/HTP and the fuselage/wings/VTP, respectively.

A. Stability and Control

Calculations of the stability and control derivatives are made running the AVL method at zero angle of attack and zero sideslip angle, altitude = 1500 m, and Mach = 0.2. The derivatives of the vertical and lateral moments coefficients with respect to the angle of attack α and the sideslip angle β, $C_{m\alpha}$, and $C_{n\beta}$ provided by the AVL method are made dimensionless with the dynamic pressure at the freestream, a wing reference area, and the mean chord of the wing. Thus, the contributions of the HTP and VTP are rescaled in the same way and they can be added to obtain the stability derivatives of the empennage. The contributions of the HTP and VTP depend on the six free parameters of the HTP, namely

$$C_{m\alpha}^{\mathrm{HTP}} = F_1(\lambda_1, \ldots, \lambda_6), \qquad C_{n\beta}^{\mathrm{HTP}} = F_2(\lambda_1, \ldots, \lambda_6) \tag{A9}$$

Since the VTP is exactly vertical, it produces no vertical force. Its contribution to the lateral force stability derivative depends on the three HTP free parameters, namely

$$C_{n\beta}^{\mathrm{VTP}} = F_3(\lambda_7, \lambda_8, \lambda_9) \tag{A10}$$

The control derivatives are made dimensionless similarly. Again, the contributions of the HTP/VTP to the control derivatives depend on associated free parameters, namely

$$C_{m\delta}^{\mathrm{HTP}} = F_4(\lambda_1, \ldots, \lambda_6), \qquad C_{n\delta}^{\mathrm{HTP}} = F_5(\lambda_1, \ldots, \lambda_6) \tag{A11}$$

$$C_{n\delta}^{\mathrm{VTP}} = F_6(\lambda_7, \lambda_8, \lambda_9) \tag{A12}$$

The functions $F_1, \ldots, F_6$ defined in Eqs. (A9–A12) are treated using as surrogate model those resulting from applying HOSVD + I to this function.

B. Stall Restrictions

These restrictions (Sec. IV.B) are imposed at altitude = 1500 m, Mach = 0.2, and $\beta = 0°$, and require (Sec. IV.B) to calculate (using AVL) the spanwise maximum (at $\alpha = 25°$) and minimum (at $\alpha = -25°$) values of the chordwise lift coefficients on the various cross sections, $Cl_{\max}$ and $Cl_{\min}$. These depend on the six free parameters that define the HTP geometry, namely

$$Cl_{\min} = F_7(\lambda_1, \ldots, \lambda_6), \qquad Cl_{\max} = F_8(\lambda_1, \ldots, \lambda_6) \tag{A13}$$

Again, these two functions are treated using as surrogate model those resulting from applying HOSVD + I to these functions.

III. Aerodynamics and Structures Ingredients

AVL calculations are performed at Mach = 0.5, altitude= 1500 m, and three combinations of the angle of attack and the sideslip angle, namely $(\alpha, \beta) = (0°, 10°)$, (10°,0°), and (5°,5°).

A. Aerodynamic Loads

AVL provides the local pressure distribution at each chordwise section of the HTP, $p(x, s)$ (in terms of the streamwise coordinate x and the arch length along the generatrix s), which is assumed as applied at the midlines surface. With this, the shear force, bending moment, and torsional moment on the span section $s = s_0$ are calculated as

$$\begin{aligned} Q(s_0) &= 1.5 \int_{s_0}^{\lambda_1+\lambda_2} \int_{x_{\mathrm{te}}(s)}^{x_{\mathrm{le}}(s)} p(x, s) \cos(\theta - \theta_0) \sin\varphi \, \mathrm{d}x \, \mathrm{d}s \\ M(s_0) &= 1.5 \int_{s_0}^{\lambda_1+\lambda_2} \int_{x_{\mathrm{te}}(s)}^{x_{\mathrm{le}}(s)} [p(x, s)(y - y_0) \cos\theta \\ &\quad + p(x, s)(z - z_0) \sin\theta] \sin\varphi \, \mathrm{d}x \, \mathrm{d}s \\ T(s_0) &= 1.5 \int_{s_0}^{\lambda_1+\lambda_2} \int_{x_{\mathrm{te}}(s)}^{x_{\mathrm{le}}(s)} p(x, s)(x - x_0) \cos(\theta - \theta_0) \\ &\quad \times \sin\varphi \, \mathrm{d}x \, \mathrm{d}s \end{aligned} \tag{A14}$$

where x_{te} and x_{le} are the x-coordinates of the trailing and leading edges of each chordwise section, respectively, and x_0 is the chordwise coordinate of the midpoint of the torsion box; $\theta - \theta_0$ is the angle between the unit normals to the midlines surface at the sections $s = s_0$ and $s = s$, which are both contained in the plane $y - z$ (see Fig. A1); and $\sin\varphi \, \mathrm{d}x \, \mathrm{d}s = \mathrm{d}A$ is the differential of area along the midlines surface, which is defined in terms of the angle φ between the tangent to the generatrix and the chordwise section (see Fig. A1). In addition, a safety factor of 1.5 is applied.

Equations (A14) must be applied to all considered configurations of the HTP, and the three above mentioned combinations of the angle of attack and the sideslip angle. Since the two pieces of the HTP must be considered independently, a total number of six distributions of Q, M, and T must be considered. These depend on s_0 and the six free parameters of the HTP, as

$$\begin{aligned} Q = Q_j(\lambda_1, \ldots, \lambda_6, s_0), \qquad M = M_j(\lambda_1, \ldots, \lambda_6, s_0) \\ T = T_j(\lambda_1, \ldots, \lambda_6, s_0) \end{aligned} \tag{A15}$$

for $j = 1, \ldots, 6$. The HOSVD + I method provides surrogates for these 18 functions. The VTP is treated similarly but the load distributions are independent of the angle of attack. Thus, only one distribution of Q, M, and T results, which depends on the vertical position of the chordwise section z_0 and the three free parameters of the HTP, as

$$\begin{aligned} Q = Q_7(\lambda_7, \lambda_8, \lambda_9, z_0), \qquad M = M_7(\lambda_7, \lambda_8, \lambda_9, z_0) \\ T = T_7(\lambda_7, \lambda_8, \lambda_9, z_0) \end{aligned}$$

Again, the HOSVD + I methodology provides surrogates for these three functions.

B. Weight

For the sake of brevity, only the HTP is considered below; the VTP is treated similarly. The main assumption is that aerodynamic loads on the HTP are completely supported by a longitudinal torsion box, which extends span wise along the HTP. The torsion box (Fig. A3) is a rectangular box formed by a leading and a trailing spars, which are located at 20 and 55% of the chord, respectively, and the cover joining both spars on their upper and lower edges, to complete the box. The height and width of the box will be denoted as h and d, respectively.

Thus, the structural elements in the torsion are the cover and the spars, whose thicknesses are to be determined. Cover thickness

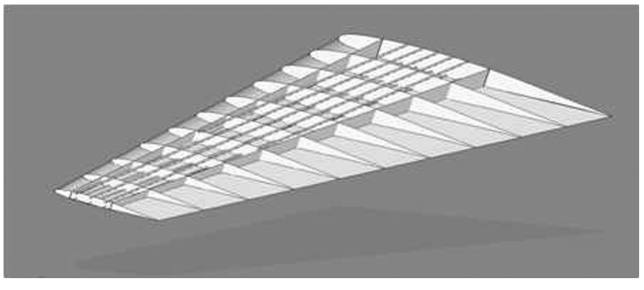

Fig. A3 The structure.

includes the actual skin thickness plus the effect of stringers. The equivalent cover thickness t is computed setting up the admissible stress σ_{adm} as that of the baseline configuration, which is $\sigma_{\text{adm}} = 360$ MPa. Assuming that the torsion box is symmetric, the stress in the upper cover can be defined in terms of the moment of inertia of the box and the bending moment calculated above, as

$$\sigma = \frac{M(s)h(s)}{2I_x(s)} \approx \frac{M(s)}{t(s)d(s)h(s)} \tag{A16}$$

where s is the arch length along the generatrix of the HTP, as above. This equation allows for calculating the thickness t (recall that both d and h are known, and M is provided by a surrogate, as described in Appendix A.III.A) along the span.

To calculate the thickness of the spars, we consider the maximum shear flow, defined as

$$q_{\max}(s) = \left|\frac{T(s)}{2d(s)h(s)}\right| + \left|\frac{Q(s)}{2h(s)}\right| \tag{A17}$$

where d is the torsion box width, T is the torsional moment, and Q is the shear force. The latter two are provided by two surrogate models, as described in Appendix A.III.A. Now, a permissible shear stress is defined as that of the baseline configuration, which is $\tau_{\text{adm}} =$ 180 MPa. The shear stress is defined as the product of the spar thickness and the shear flow. The resulting spar thickness is

$$t_{\text{sp}}(s) = \frac{q_{\max}}{\tau_{\text{adm}}} \tag{A18}$$

where $q_{\max}$ is as calculated above. Finally, no matter what the outcome of the computation above is, the minimum thickness considered in every component is 2.5 mm.

Once the thickness of the structure has been calculated, the weight of each HTP weight is calculated as

$$\text{Weight} = 2\int_{S_{\text{TB}}} \frac{\rho_{\text{cov}}\,\text{dA}\,t_{\text{cov}}(s) + \rho_{\text{sp}}h(s)t_{\text{sp}}(s)}{c(s)}\,\text{d}S + \rho_s\left(A_S - \int_{S_{\text{TB}}} \frac{d(s)}{c(s)}\,\text{d}A\right) \tag{A19}$$

where the first term yields both the weight of the equivalent upper and lower panels of the box and spars weight, and the second term accounts for the remaining stabilizer. In these integrals, S_{TB} is that part of the mean-lines surface of the HTP occupied to the torsion box, A_S is the total area of the mean-lines surface, and $\text{d}A = \sin\varphi\,\text{d}x\,\text{d}s$ is the differential of area along the midlines surface, as above; ρ_{cov} and ρ_{sp} are the skin and spars material density, respectively, and ρ_s is the density per unit surface of the stabilizer part that is not torsion box, defined in such a way that it accounts for the weight of other components and mechanical parts.

Acknowledgment

This research has been partially funded by the Spanish Ministry of Education, under Grants DPI2009-07591 and TRA 2007-65699. We are also in debt to two anonymous referees for various useful comments on an earlier version of the article.

References

[1] Price, M., Raghunathan, S., and Curran, R., "An Integrated Systems Engineering Approach to Aircraft Design," *Progress in Aerospace Sciences*, Vol. 42, No. 4, 2006, pp. 331–376. doi:10.1016/j.paerosci.2006.11.002

[2] Antoine, N. E., and Kroo, I., "Aircraft Optimization for Minimal Environmental Impact," *Journal of Aircraft*, Vol. 41, No. 4, 2004, pp. 790–797. doi:10.2514/1.71

[3] Antoine, N. E., and Kroo, I., "Framework for Aircraft Conceptual Design and Environmental Performance Studies," *AIAA Journal*, Vol. 43, No. 10, 2005, pp. 2100–2109. doi:10.2514/1.13017

[4] Nelder, J. A., and Mead, R., "A Simplex Method for Function Minimization," *Computer Journal*, Vol. 7, No. 4, 1965, pp. 308–313.

[5] Piperni, P., Abdo, M., and Kafyeke, F., "The Application of Multi-Disciplinary Optimization Technologies to the Design of a Business Jet," *10th AIAA/ISSMO Multidisciplinary Analysis and Optimisation Conference*, AIAA 2004-4370, Aug. 2004.

[6] Schumacher, G., Murra, I., Wang, L., Laxander, A., O'Leary, O., and Herold, M., "Multidisciplinary Design Optimization of a Regional Aircraft Wing Box," *9th AIAA/ISSMO Multidisciplinary Analysis and Optimisation Conference*, AIAA 2002-5406, Sept. 2002.

[7] Bower, G., and Kroo, I., "Multi-Objective Aircraft Optimization for Minimum Cost and Emissions Over Specific Route Networks," *ICAS 2008, 26th International Conference of the Aeronautical Sciences*, IEEE Publications, Piscataway, NJ, 2008.

[8] Rao, C., Ray, T., and Tsai, H., "Aircraft Configuration Design Using a Multidisciplinary Optimization Approach," *42nd AIAA Aerospace Sciences Meeting and Exhibit*, AIAA 2004-536, Jan. 2004.

[9] Choi, S., Alonso, J., and Kroo, I., "Multifidelity Design Optimization of Low-Boom Supersonic Jets," *Journal of Aircraft*, Vol. 45, No. 1, 2008, pp. 106–118. doi:10.2514/1.28948

[10] Werner–Westphal, C., Heinze, W., and Horst, P., "Multidisciplinary Integrated Preliminary Design Applied to Future Green Aircraft Configurations," *45th Aerospace Sciences Meeting and Exhibit*, AIAA Paper 2007-655, Jan. 2007.

[11] Forrester, A. I. J., and Keane, A., "Recent Advances in Surrogate-Based Optimization," *Progress in Aerospace Sciences*, Vol. 45, Nos. 1–3, 2009, pp. 50–79. doi:10.1016/j.paerosci.2008.11.001

[12] Queipo, N. V., Haftka, R. T., Shyy, W., Goel, T., Vaidyanathan, R., and Tucker, P. K., "Surrogate-Based Analysis and Optimization," *Progress in Aerospace Sciences*, Vol. 41, No. 1, 2005, pp. 1–28. doi:10.1016/j.paerosci.2005.02.001

[13] Kroo, I., Altus, S., Braun, R., Gage, P., and Sobieski, I., "Multidisciplinary Optimization Methods for Aircraft Preliminary Design," *5th AIAA/USAF/NASA/ISSMO Symposium on Multidisciplinary Analysis and Optimization*, AIAA Paper 94-4325, Sept. 1994.

[14] Roth, B., and Kroo, I., "Enhanced Collaborative Optimization: A Decomposition Based Method for Multidisciplinary Design," *Proceedings of the ASME 2008 International Design Engineering Technical Conferences and Computers and Information in Engineering Conference*, American Society of Mechanical Engineers, Fairfield, NJ, Aug. 2008.

[15] Legresley, P., and Alonso, J., "Improving the Performance of Design Decomposition Methods with POD," *10th AIAA/ISSMO Multidisciplinary Analysis and Optimization Conference*, AIAA Paper 2004-4465, Aug. 2004.

[16] Chacksfield, J. E., "Multivariate Optimization Techniques and Their Impact on the Aircraft Design Process," *Progress in Aerospace Sciences*, Vol. 33, Nos. 11–12, 1998, pp. 731–757. doi:10.1016/S0376-0421(97)00011-0

[17] Jameson, A., "A Perspective on Computational Algorithms for Aerodyanmics Analysis and Design," *Progress in Aerospace Sciences*, Vol. 37, No. 2, 2001, pp. 197–243. doi:10.1016/S0376-0421(01)00004-5

[18] Hajela, P., "Soft Computing in Multidisciplinary Aerospace Design: New Directions for Research," *Progress in Aerospace Sciences*, Vol. 38, No. 1, 2002, pp. 1–21. doi:10.1016/S0376-0421(01)00015-X

[19] Lian, Y., Oyama, A., and Liou, M.-S., "Progress in Design Optimization Using Evolutionary Algorithms for Aerodynamics Problems," *Progress in Aerospace Sciences*, Vol. 46, 2010, pp. 199–223. doi:10.1016/j.paerosci.2009.08.003

[20] Berard, A., and Isikveren, A. T., "Conceptual Design Prediction of the Buffet Envelope of Transport Aircraft," *Journal of Aircraft*, Vol. 46, No. 5, 2009, pp. 1593–1606. doi:10.2514/1.41367

[21] Golub, G. H., and Van Loan, G. T., *Matrix Computations*, John Hopkins Univ. Press, College Park, MD, 1996.

[22] da Silva, V., and Lim, L. H., "Tensor Rank and the Ill-Posedness of the Best Low-Rank Approximation Problem," *SIAM Journal on Matrix Analysis and Applications*, Vol. 30, No. 3, 2008, pp. 1084–1127. doi:10.1137/06066518X

[23] de Lathauwer, L., de Moor, B., and Vandewalle, J., "On the Best Rank-One and Rank-$(R_1, R_2, \ldots, R_N)$ Approximation of Higher Order Tensors, Between the Six Flow Variables," *SIAM Journal on Matrix Analysis and Applications*, Vol. 21, No. 4, 2000, pp. 1324–1342. doi:10.1137/S0895479898346995

[24] Kolda, T. G., and Bader, B. W., "Tensor Decompositions and Applications," *SIAM Review*, Vol. 51, No. 3, 2009, pp. 455–500. doi:10.1137/07070111X

[25] de Lathauwer, L., de Moor, B., and Vandewalle, J. "A Multilinear Singular Value Decomposition," *SIAM Journal on Matrix Analysis and Applications*, Vol. 21, No. 4, 2000, pp. 1253–1278. doi:10.1137/S0895479896305696

[26] Lorente, L. S., Vega, J. M., and Velazquez, A., "Compression of Aerodynamic Databases Using Singular Value Decomposition," *Aerospace Science and Technology*, Vol. 14, No. 3, 2010, pp. 168–177. doi:10.1016/j.ast.2009.12.003

[27] Alonso, D., Velazquez, A., and Vega, J. M., "A Method to Generate Computationally Efficient Reduced Order Models," *Computer Methods in Applied Mechanics and Engineering*, Vol. 198, 2009, pp. 2683–2691. doi:10.1016/j.cma.2009.03.012

[28] Eddy, J., and Lewis, K., "Effective Generation of Pareto Sets Using Genetic Programming," *ASME 2001 Design Engineering Technical Conferences and Computers and Information in Engineering Conference*, American Society of Mechanical Engineers Paper DETC2001/DAC-21094, Sept. 2001.

[29] Ferguson, S., Gurnani, A., Donndelinger, J., and Lewis, K., "A Study of Convergence and Mapping in Multiobjective Optimization Problems," *ASME 2005 Design Engineering Technical Conferences and Computers and Information in Engineering Conference*, American Society of Mechanical Engineers Paper DETC2005-84852, Sept. 2005.

[30] Astrid, P., Weiland, S., Willcox, K., and Backx, T., "Missing Point Estimation Methods in Models Described by Proper Orthogonal Decomposition," *IEEE Transactions on Automatic Control*, Vol. 53, 2008, pp. 2237–2250. doi:10.1109/TAC.2008.2006102

[31] Braconnier, T., Ferrier, M., Jouhaud, J. C., Montagnac, M., and Sagaut, P., "Towards an Adaptive POD/SVD Surrogate Model for Aeronautic Design," *Computers and Fluids*, Vol. 40, 2011, pp. 195–209. doi:10.1016/j.compfluid.2010.09.002

[32] Schilchting, H., *Boundary Layer Theory*, McGraw–Hill, New York, 1979.

K. Willcox
Associate Editor